Marine Geology 336 (2013) 24–32

Contents lists available at SciVerse ScienceDirect

Marine Geology

journal homepage: www.elsevier.com/locate/margeo

Observations of suspended sediment stratification from acoustic backscatter in muddy environments

Cihan Sahin [a,*], Ilgar Safak [b], Tian-Jian Hsu [c], Alexandru Sheremet [a]

[a] Department of Civil and Coastal Engineering, University of Florida, Gainesville, FL, USA
[b] Department of Environmental Sciences, University of Virginia, Charlottesville, VA, USA
[c] Center for Applied Coastal Research, Department of Civil and Environmental Engineering, University of Delaware, Newark, DE, USA

ARTICLE INFO

Article history:
Received 27 June 2012
Received in revised form 30 November 2012
Accepted 2 December 2012
Available online 9 December 2012

Communicated by J.T. Wells

Keywords:
suspended sediment
cohesive sediment
sediment stratification
wave–sediment interaction
mud
bottom boundary layer
Louisiana Shelf

ABSTRACT

Vertical profiles of suspended sediment concentration estimated from acoustic backscatter are used to re-examine the relation between sediment stratification and floc size in a cohesive sedimentary environment. Concentration measurements by optical backscatter sensors at two vertical levels are used to calibrate the acoustic backscatter intensity. In spite of the complexities due to the rapidly changing flow and cohesive sediment properties, the estimates of sediment concentration reproduce well the observations. Together with the vertical profiles of suspended sediment concentration, measured current profiles are used to calibrate a one-dimensional-vertical (1DV) boundary layer numerical model for combined wave–current flow on muddy beds. The numerical simulations are used to investigate the effect of the floc size on the vertical structure of the suspended sediment concentration profile. For similar flow conditions, smaller flocs result in more mixed profiles with higher concentration in the upper water column and lower near-bed concentration. This is the first time this effect is seen in direct field observations, and confirms previously published numerical results.

1. Introduction

Acoustic profilers have been used successfully in recent years for estimating the vertical structure of suspended sediment concentration (SSC) in sandy environments. They provide high temporal and spatial resolution, can be deployed in high energy conditions (when traditional water sampling becomes difficult) and do not distort the flow, as the measurements are collected at distance (Lynch et al., 1991; Hay and Sheng, 1992; Thorne et al., 1993; Thosteson and Hanes, 1998; Holdaway et al., 1999; Thorne and Hanes, 2002). To observe near-bed sediment transport, the instrument is typically mounted at about 1–2 mab (meter above bed), and transmits a high-frequency sound signal toward the bed. The signal reflected by sediment suspended at different elevations can be related to sediment concentration (Thorne and Hanes, 2002). The analysis is complicated by the strong dependency of the acoustic scattering processes on instrument characteristics, as well as environmental factors, such as sediment concentration, structure, and specifics of sediment–sound interaction.

Efforts to apply this methodology in mud-dominated environments have been hampered by the additional complexities of cohesive sediment characteristics (e.g., variable particle size and density due to the floc formation and breakup) that are strongly correlated to flow turbulence and amount of sediment in suspension. Recent studies (Gartner, 2004; Hoitink and Hoekstra, 2005; Ha et al., 2011) focused on the performance of acoustic profilers in dilute cohesive sediment concentrations (up to the order of 0.1 g/L). It is still unclear how accurate these methods are in higher concentrations and/or high concentration-gradient conditions (e.g., lutocline and fluid mud layer). Hamilton et al. (1998) used an acoustic profiler to estimate SSC in solutions of up to 10 g/L; however, their estimates were not compared with independent concentration measurements.

In muddy environments, vertical profiles of SSC are typically estimated using numerical models (e.g., Winterwerp, 2001, 2002; Hsu et al., 2009) that take as input a small number of point measurements of SSC (for example, derived from calibrated optical sensors deployed at different heights above the bed). These models are essential for studying flow-related parameters that are difficult to measure directly, such as near-bed turbulent stresses. The quality and resolution of the observational data used to drive these models is a major concern. For example, Safak et al. (2010) showed that a limited vertical resolution (1–2 point measurements) can be matched with the model with different vertical profiles, i.e., using different model parameters (e.g., different settling velocity or floc size). The values of the parameters needed to calibrate the model in this case are not uniquely defined. The availability of high-resolution SSC profiles is therefore critical for properly constraining numerical simulations and understanding

* Corresponding author. Tel.: +1 352 392 9537x1410; fax: +1 352 392 3394.
E-mail addresses: cisahin@ufl.edu (C. Sahin), safak@virginia.edu (I. Safak), thsu@udel.edu (T.-J. Hsu), alex@coastal.ufl.edu (A. Sheremet).

0025-3227/$ – see front matter © 2012 Elsevier B.V. All rights reserved.
http://dx.doi.org/10.1016/j.margeo.2012.12.001

the physics of the boundary layer hydrodynamics–sediment interaction. Another aspect of numerical modeling is result validation. Safak et al. (2010) studied numerically the effect of floc size on the vertical SSC profile and inferred that decreasing floc size, which results in a decrease in settling velocity, produces more mixed concentration profile with smaller near-bed sediment concentration. Since the relationship between floc size and settling velocity, and the associated attenuation of turbulence through sediment-induced density stratification are part of the model closures, this result still needs confirmation based on more comprehensive field observations.

In this study, near-bed sediment and hydrodynamic observations collected in 2006 on the muddy Atchafalaya Shelf, Louisiana, USA (Section 2) are used to develop and validate a method to estimate vertical profiles of SSC from the acoustic backscatter of current profilers (Section 3) in relatively high concentrations (up to 10 g/L). The high-resolution SSC profile estimates are used in Section 4 to constrain a wave–current boundary layer model for cohesive beds (Hsu et al., 2009), and to investigate the role of the floc size on vertical SSC profile. The results are discussed in Section 5 and the conclusions are summarized in Section 6.

2. Field experiment

2.1. Site and instrumentation

The data set used in this study was collected between March 3rd and March 9th, 2006, on the muddy inner shelf fronting the Atchafalaya Bay, Louisiana, USA, as part of a larger-scope study of hydrodynamics and sediment transport processes in shallow muddy environments. A description of the field conditions during the 2006 experiment can be found in Jaramillo et al. (2009). Briefly, the Atchafalaya Shelf is wide and shallow (the 10-m isobath is about 40 km offshore) with a slope of less than 1:1000. The sub-aqueous feature on the muddy inner shelf fronting the bay is defined as a clinoform of up to 3-m thick mud layer (Neill and Allison, 2005; Jaramillo et al., 2009). The inner shelf receives about 30% of the discharge of the Mississippi River, i.e., approximately 84 million metric tons of sediment, annually (Mossa, 1996), with a representative grain-size at the site ranging between 2 and 7 μm, with 17% fine-sand content (Allison et al., 2000, 2005; Sheremet et al., 2005; Safak et al., 2010). This study focuses on observations collected by an instrumented platform deployed near the 4-m isobath (Fig. 1a, also platform "T2", "Experiment A" in Jaramillo et al., 2009) which also included observations of sediment-size distribution, in addition to wave–current observations and optical backscatter SSC observations.

The schematic of the configuration of the instrumented platform is shown in Fig. 1b. Near-bed current velocities were measured using a downward-pointing, 1500-kHz PC-ADP (Pulse-Coherent Acoustic Doppler Profiler, manufactured by Sontek/YSI) which uses three beams oriented 15° off the vertical axis. The PC-ADP sampled at 2 Hz in 60 bins of 2 cm, following a 10-cm blanking distance in 10-min bursts every 30 min. The PC-ADP also logged SSC observations collected by two synchronized OBS-3s (Optical Backscatterance Sensors, D&A Instruments, Campbell Sci.) mounted at 50 and 75 cmab (cm above the bed). The OBS-3s were calibrated in the laboratory using sediment and water samples collected at the experiment site. Grain-size distributions of suspended sediments were estimated based on the observations of a LISST-100X Type-C (Laser In Situ Scattering Transmissometer, Sequoia Scientific) mounted at 120 cmab which estimates size distributions of suspended particles (flocs and primary) at 32 class ranges between 2.5 and 500 μm. The instrument recorded the grain-size distribution of suspended sediment every minute (average of 100, 2-Hz samples) in 30-min bursts each hour.

The PC-ADP pressure time series segments of 10-min length were de-trended and de-meaned, then divided into 128 s blocks with 50% overlap, and tapered using a Hanning window. The resulting spectra have approximately 17 degrees of freedom. The significant wave-height H_s was estimated based on the relation $H_s^2 = 16 \int_{f_1}^{f_2} S_{\eta\eta}(f)\, df$ where $S_{\eta\eta}$ is the power spectral density of sea surface elevation η at frequency f, estimated using standard spectral analysis. $S_{\eta\eta}$ was corrected for depth attenuation using the linear wave theory, with a high-frequency cutoff defined by a depth attenuation of wave variance larger than 95%. A spectral tail proportional to f^{-5} was added to cover the high frequency range (Phillips, 1958). Swell (long waves) and sea (short waves) bands were distinguished by using a cutoff frequency of $f_c = 0.2$ Hz, e.g., for swell band $f_1 = 0.0078$ Hz, $f_2 = f_c$; for sea band $f_1 = f_c$, $f_2 = 0.992$ Hz. Representative flow and sediment statistics (mean speed and direction of currents, wave spectrum, significant wave height, and mean concentration) were calculated for 30-min intervals, resulting in a 281-point time series of mean values for PC-ADP and OBS data. The measurement interval for the LISST data was 1 h (a total of 141 mean-value observations).

2.2. Observations

Observed 30-min averages of significant wave height, current speed and direction, backscatter profiles, and SSC observations are shown in Fig. 2. Until March 8th, 17:00, the swell energy was much lower than the energy of seas (Fig. 2a). The location of the maximum backscatter, which is assumed to be the sea bed position throughout this study, was steady during this period (intense black line in Fig. 2d), suggesting

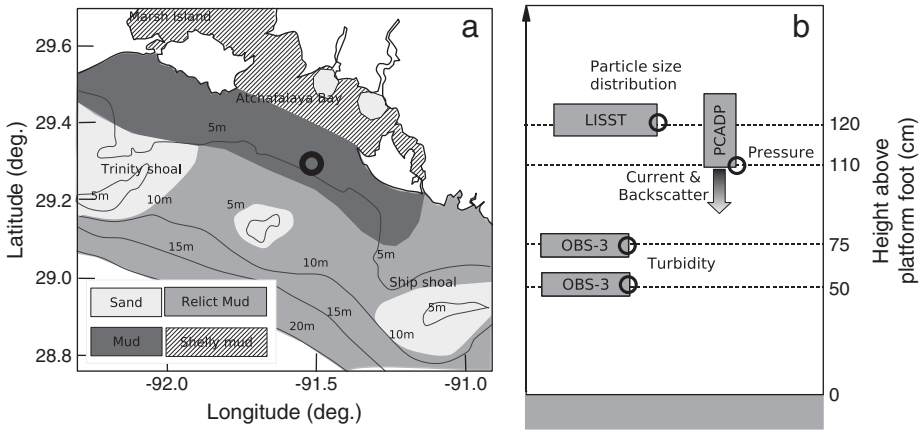

Fig. 1. (a) The approximate distribution of the surficial sediments on the Atchafalaya Shelf (Neill and Allison, 2005; Jaramillo et al., 2009). The circle marks the location of the instrumented platform (29.26° latitude North, 91.57° longitude West). (b) Configuration of the instruments. Circles mark the location of the sampling volumes of point measurements, arrows indicate the profiler's direction of acoustic signal transmission.

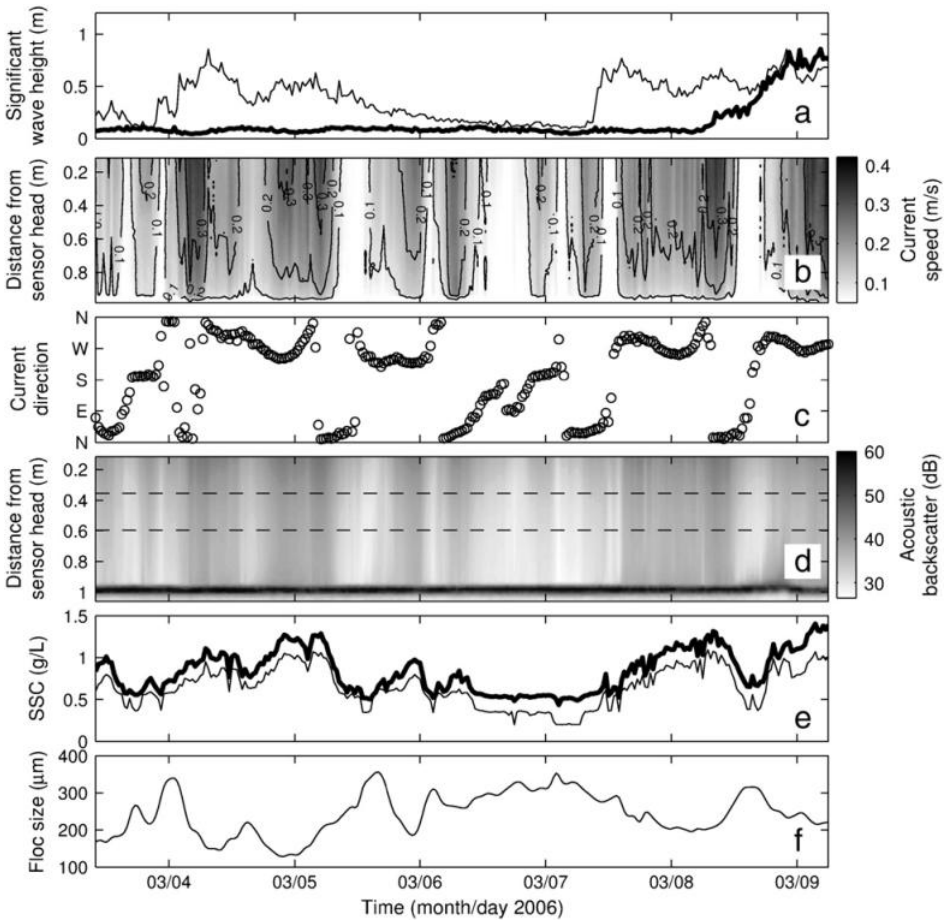

Fig. 2. Time evolution of (a) significant wave height at the surface in the sea ($f > 0.2$ Hz, thin line) and swell ($f \leq 0.2$ Hz, thick line) bands; the PC-ADP measurements of (b) current speed profiles (c) vertically averaged current directions; (d) normalized acoustic backscatter intensity (dashed lines correspond to the elevations at which the OBS-3s were sampling); (e) suspended sediment concentration measured by the OBS-3s (thick line: 50 cmab, thin line: 75 cmab); (f) mean floc size measured by the LISST.

negligible bed reworking by waves and currents. However, a small amount of sediment must have been available for mobilization on the shelf, as the evolution of SSC values measured by the OBSs largely followed the variations of sea energy (Fig. 2a and e), and current speed and direction. (Fig. 2b and c). An increase in the swell energy starting on March 8th appears eventually to have triggered some bed evolution (slight change in maximum backscatter location, Fig. 2d), together with increasing SSC values (Fig. 2e). The grain-size distribution estimated from the LISST measurements was bimodal with a dominant floc-mode around 230 μm and a weaker floc-mode positioned around 50 μm (Safak et al., 2010). The mean floc size extracted from the grain size distribution varied between 100 μm and 300 μm with the average around 200 μm (Fig. 2f).

3. Conversion of acoustic backscatter to SSC

3.1. Conversion algorithm

For spherical particles, Sheng and Hay (1988), and later Thorne et al. (1993); Holdaway et al. (1999); Thorne and Hanes (2002) showed that the vertical profile of suspended sediment concentration, $SSC(r)$ can be determined from the backscatter intensity of an acoustic profiler (in this study, the PC-ADP, see Fig. 1b) as

$$SSC(r) = \left(\frac{V(r) r \psi}{k_s k_t}\right)^2 e^{4r\alpha}, \tag{1}$$

where r is the slant range along the axis to the insonified volume, $V(r)$ is the recorded voltage converted to backscatter strength in dB, and ψ is the near-field correction factor that describes the departure from spherical spreading in the near-field of the transducer (Downing et al., 1995); k_t is a system constant, and α denotes the attenuation coefficient. The scattering properties of the sediments are represented by the parameter

$$k_s = \frac{\langle f_f \rangle}{\sqrt{\langle a \rangle \rho}}, \tag{2}$$

where f_f is the form function that describes the scattering characteristics of particles in suspension, a is the radius of the sediment in suspension, and ρ is the sediment density. The angular brackets represent the average over the particle-size distribution. The attenuation coefficient $\alpha = \alpha_w + \alpha_s$ has a water component α_w which is a function of acoustic frequency, water temperature, depth, and salinity (e.g., Francois and Garrison, 1982a,b; Kaye and Laby, 1986), and a sediment component α_s. The latter can be calculated (Urick, 1948; Thorne and Hanes, 2002) as

$$\alpha_s = \frac{1}{r}\int_0^r (\xi_s + \xi_v)\, SSC(R) dR, \tag{3}$$

and depends on two critical parameters: the attenuation ξ_s due to scattering particles; and a frictional loss ξ_v due to the viscosity of the fluid surrounding the particles. The scattering loss ξ_s is written as (Thorne and Hanes, 2002)

$$\xi_s = \frac{3}{4\langle a \rangle \rho} \langle \chi \rangle, \tag{4}$$

with χ the normalized total scattering cross-section. The parameters χ and f_f can be calculated using the simplified expressions given based on the measurements of these parameters for sediment suspensions and individual irregularly shaped particles from several sources (Sheng and Hay, 1988; Crawford and Hay, 1993; Thorne et al., 1993; Thorne and Meral, 2008). The viscous absorption is calculated as follows (Urick, 1948)

$$\xi_v = \frac{k(\sigma-1)^2 s}{2\rho\{s^2+(\sigma+\delta)^2\}}, \tag{5}$$

with

$$s = \frac{9}{4\beta a}\left[1+\frac{1}{\beta a}\right];\quad \sigma = \frac{\rho}{\rho_w};\quad \text{and}\quad \delta = \frac{1}{2}\left[1+\frac{9}{2\beta a}\right],\quad \text{with}\quad \beta = \sqrt{\frac{\omega}{2\nu}}.$$

Here, k is the wave number of the acoustic signal, ρ_w denotes the water density, $\omega = 2\pi f$ with f being the acoustic frequency, ν is the kinematic viscosity of water. In this study, flocs are assumed to be the scatterers and contribute to the scattering loss ξ_s while single cohesive sediment particles forming flocs contribute to the viscous part of the attenuation ξ_v (see discussion in Section 5).

The sediment absorption α_s can be calculated for known SSC profiles. If the SSC profile is not known, for dilute concentrations α_s can be assumed negligible (Thorne and Hanes, 2002). However, in high concentrations (e.g., >1 g/L) such as those observed in this study (Section 2), α_s has to be taken into account. The resulting implicit problem can be solved for $SSC(r)$ using an iterative approach (e.g., Thorne and Hanes, 2002). The following steps are applied to calculate SSC profiles. In Eq. (1), the slant range is determined for each measurement bin as a function of transducer angle, bin size and blanking distance. The near field correction ψ is calculated following Downing et al. (1995); the water absorption factor α_w is tabulated (e.g., Francois and Garrison, 1982a,b). If sediment size information is available, the density of mud flocs is estimated following Kranenburg (1994) as

$$\rho = \rho_w + (\rho_s - \rho_w)\left[\frac{D_p}{D_f}\right]^{3-n_f}, \tag{6}$$

where ρ, ρ_w and ρ_s are the densities of mud flocs, water and primary sediment particles, and D_f and D_p are floc and primary particle diameters, respectively. The exponent is a function of the fractal dimension n_f of the floc. Eqs. (2), (4) and (5) can then be used to calculate the parameters k_s, ξ_s (setting, e.g., $a = D_f/2$) and ξ_v (setting, e.g., $a = D_p/2$).

Standard methods for determining the instrument constant k_t (Thorne and Hanes, 2002; Betteridge et al., 2008) involve either performing a full electronic and acoustic calibration of the system, that require special equipment, or conducting extensive measurements in a homogeneous suspension with known sediment concentrations and scattering characteristics, again, requiring a special laboratory setup. In the absence of the means to perform these tests, we propose here an optimization approach that seeks to identify the value of k_t that best reproduces a selected set of observations. The optimal value of k_t results in SSC values (Eq. (1)) that minimizes the RMS error

$$\epsilon = \sqrt{\frac{1}{qN}\sum_{i=1}^{q}\sum_{j=1}^{N}\left(SSC_{OBS}^{i,j} - SSC_{AB}^{i,j}\right)^2}, \tag{7}$$

where q is the number of OBSs (optical sensors), N is the number of observations in the SSC time series, $SSC_{AB}^{i,j}$ denotes the concentration estimated based on the acoustic backscatter (AB) and $SSC_{OBS}^{i,j}$ is the measured sediment concentration at the location of ith OBS in jth measurement interval. Finally, sediment concentration at each bin is calculated using Eq. (1) using the optimal value of k_t.

3.2. Application to field observations

The application of the above algorithm to field observations requires information about sediment structure. Some parameters can be derived from LISST observations: for example, LISST estimates suggest an average of mean floc size of approximately 200 μm (Fig. 5a, Safak et al., 2010). Others, such as the floc fractal-dimension needed to evaluate Eq. (6), cannot be measured directly and were assumed to have standard values ($n_f = 2.3$ for $D_f = 200$ μm, Khelifa and Hill, 2006; Safak et al., 2010).

The one-hour LISST observations were interpolated for use with the half-hour PC-ADP and OBS measurements. In the following, we assume that the floc size is invariant with the depth, and will interpret this value as an equivalent, in some sense vertically averaged, floc size (effective size value).

The system constant, k_t, does not depend on range, particle size and concentration (Betteridge et al., 2008). SSC measurements at two vertical levels were divided into groups of 0.1 g/L (Fig. 3a). For each group, the optimum k_t giving the minimum difference between measurements and calculations was determined (Eq. (7), Fig. 3b). The value of k_t for different SSC classes does not show a significant trend and lies around the average value of 44 dB $m^{3/2}$ with the exception of the value corresponding to SSC = 0.2 g/L. That value was considered as an outlier due to measurement error and was not taken into account in calculation of k_t. Dependency of k_t on different floc size classes (25 μm intervals) is seen in Fig. 4. Again, no systematic variation is apparent. Consistent with the SSC dependency, the values lie within ±10% of the average value. The system constant k_t did not show a dependency on range, either (see "x"s and circles in Figs. 3b and 4b). Therefore, this consistent mean value of k_t was used in SSC calculations.

The values of SSC estimated from backscatter showed a good agreement with the OBS-3 observations ("x"s in Fig. 5b and c, gray "x"s in Fig. 6a, correlation coefficient $r = 0.87$ and $\varepsilon = 0.14$ g/L). In addition to the calculations using the measured floc sizes, the optimum floc sizes (also assumed vertically constant) providing the best SSC calculations at the OBS locations were obtained (circles in Figs. 5a,b and c; and 6a). Note that the LISST measurements of floc size were collected at 120 cmab while SSC measurements were at 50 and 75 cmab. This is likely to be the reason why the LISST measurements do not show strong correlation with optimum floc sizes (Fig. 6b). However, it is encouraging that optimum floc size values are in the same order of magnitude and show a similar trend with the mean floc sizes measured (Figs. 5a and 6b). This result suggests that the effective floc size D_f and SSC can be estimated when in-situ particle size measurements are not available. Fig. 5d shows the time evolution of the vertical profiles of suspended sediment concentration. Although the backscatter structure itself is often considered (and interpreted as) a meaningful representation of the SSC profile (e.g., Jaramillo et al., 2009), comparing Figs. 2d and 5d shows that the total backscatter intensity is a good indicator of the overall amount of sediment in suspension, but not of the vertical distribution of sediment.

4. Effect of floc size on concentration profiles

Safak et al. (2010) recently investigated the effect of floc size on the suspended sediment concentration profile based on numerical simulations. A part of their study held flow conditions fixed and searched for the floc size that matched point-measurements, one for SSC (at 12 cmab), and two for velocity (at 17 and 145 cmab). Their results consistently suggest that smaller floc sizes result in higher SSC values in the upper water column (more mixed profile). The possibility of estimating the entire SSC vertical profile allows us to revisit these ideas, this time from an observational standpoint. The observations are also modeled numerically to show that SSC profiles derived from acoustic backscatter can help validate the numerical models

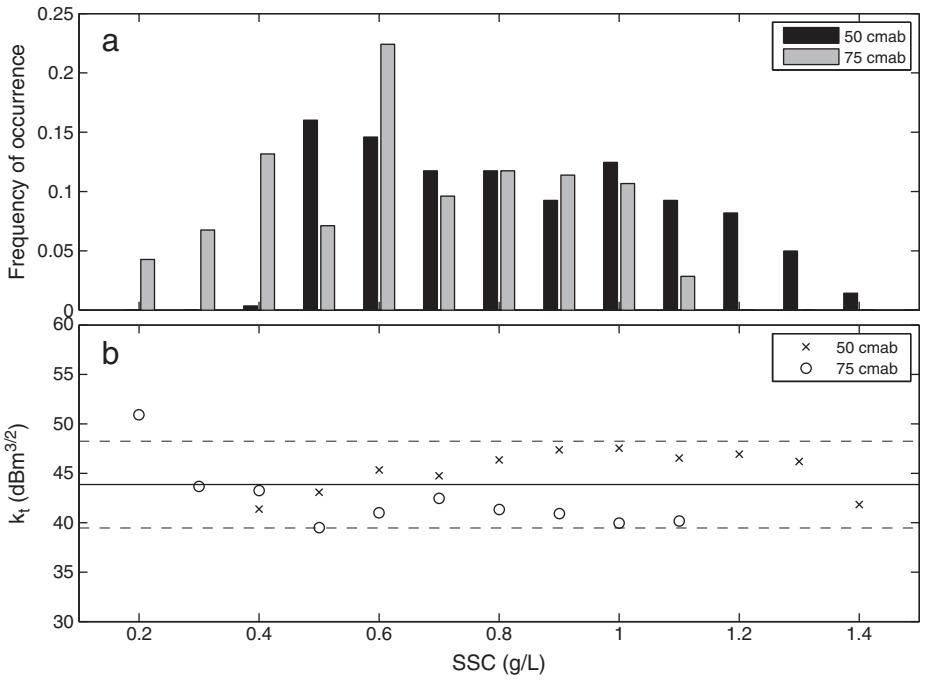

Fig. 3. (a) The histogram of suspended sediment concentration for a total of 281 mean-value observations at 50 cmab (black) and 75 cmab (gray). (b) Variation of k_t with suspended sediment concentration. Circles and "x"s denote the values at 75 cmab and 50 cmab, respectively. The solid line is the averaged k_t value over the all concentration classes and the dashed lines are ±10% difference from the average value.

and, implicitly, improve model estimates of quantities that are difficult to observe directly, such as the near-bed turbulent stress field. The model estimates of vertical turbulent intensity profiles are used in the detailed floc size–SSC profile investigation.

4.1. Numerical simulations

The observations were modeled using a 1DV (vertical domain at a single point on the horizontal plane) wave-phase-resolving bottom boundary layer numerical model developed by Hsu et al. (2009). The model, a time-dependent RANS (Reynolds-averaged Navier–Stokes) formulation based on a two-equation $k-\varepsilon$ closure, has been applied successfully in recent years to cohesive sediments (see, e.g., Hsu et al., 2007, 2009; Safak et al., 2010, 2012; Son and Hsu, 2011; Sahin et al., 2012). Suspended sediment dynamics are modeled using advection–diffusion equation coupled with the flow equations, that accounts for sediment-induced density stratification effects. The sediment phase is defined in the model by floc density (Eq. (6)), and thus by the primary

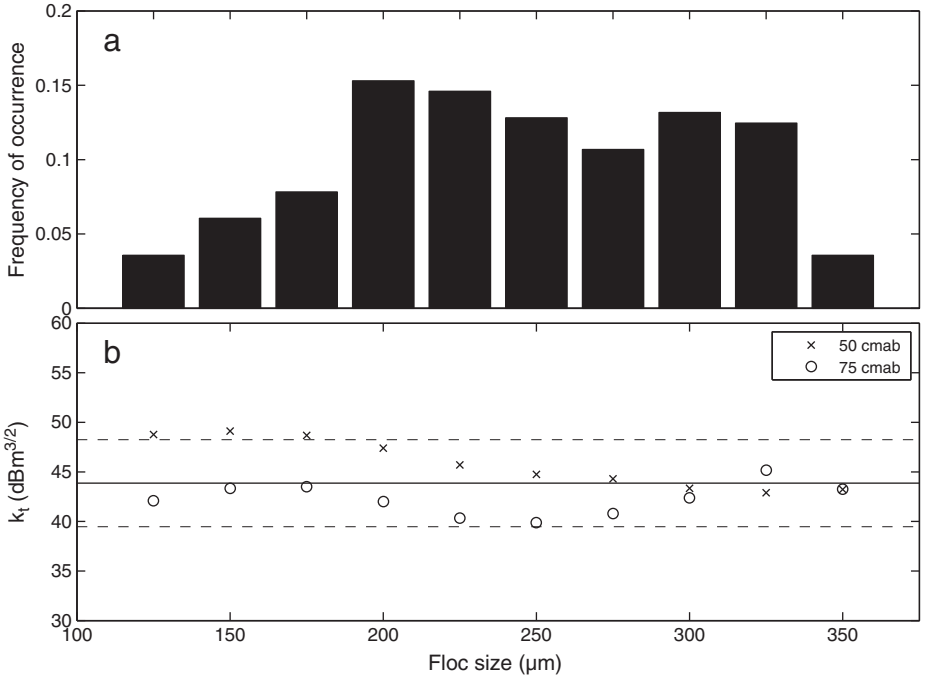

Fig. 4. (a) The histogram of floc size observations. (b) Variation of k_t with floc size. Circles and "x"s denote the values at 75 cmab and 50 cmab, respectively. The solid line is the same average value with Fig. 3b and the dashed lines are ±10% difference from the average value.

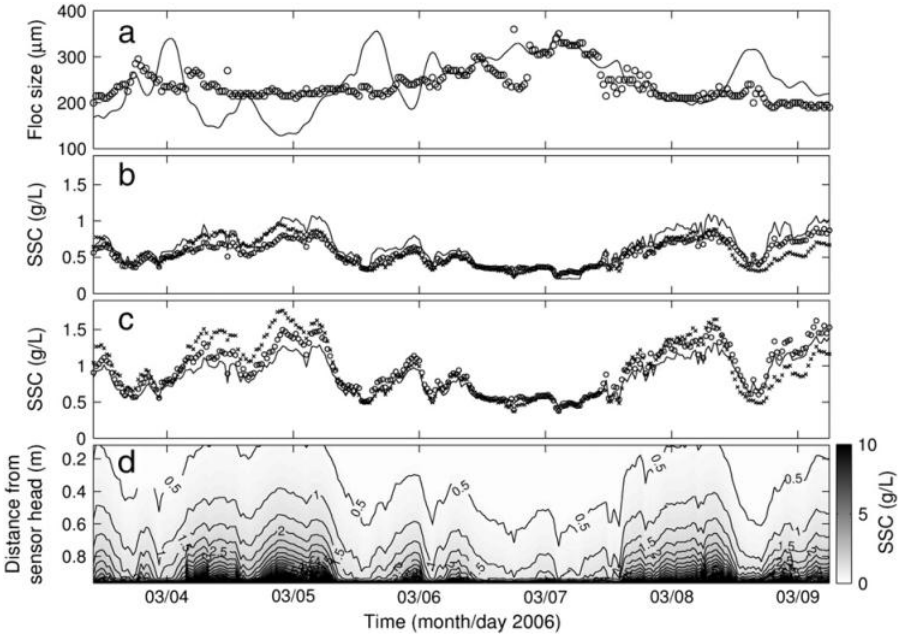

Fig. 5. Time evolution of (a) mean floc size (continuous line) and the optimum floc size yielding the best concentration estimates (circles). Suspended sediment concentration at the location of the OBSs (b) 75 cm and (c) 50 cmab (OBS — continuous line; PC-ADP estimates using mean floc size — "x"s; PC-ADP estimates using optimum floc size — circles); (d) PC-ADP derived suspended sediment concentration profiles.

particle size, floc size, and floc fractal dimension (assumed constant). Settling velocity is modeled using the Stokes law with hindered settling effect incorporated,

$$w_s = \frac{(\rho_s - \rho_w) g D_p^{3-n_f} D_f^{n_f - 1}}{18\mu}\ , \tag{8}$$

where μ is the dynamic viscosity of the fluid and g is the gravitational acceleration. Sediment availability is controlled through the resuspension coefficient (γ_o) and the critical shear stress near the bed (τ_c).

For numerical simulation purposes, the bottom location was defined as that of the maximum acoustic backscatter intensity. In its present implementation, the model assumes zero-shear at the top boundary; to satisfy this requirement and also to allow the model to match SSC estimates at the topmost PC-ADP bin (sometimes exceeding 0.6 g/L) the computational domain was extended from the bed to approximately 30 cm above the first PC-ADP bin (overall span of 1.2 m). The 2-cm vertical resolution used is equal to the PC-ADP bin height. Test runs with a 1-cm vertical resolution showed no model sensitivity to grid size, suggesting that the current boundary-layer flow dominates the processes, well resolved at a 2-cm grid size.

Sediment availability from the bed (parameter γ_o) together with roughness height (k_s) were adjusted to match estimated SSC values and measured current profiles. Because previous applications did not show model sensitivity to critical shear stress values (Hsu et al., 2009; Safak et al., 2010), this parameter was set to $\tau_c = 0.4$ Pa. This is also within the range of 0.05–1.1 Pa suggested by Hsu et al. (2007) and Hsu et al. (2009), and used by Safak et al. (2010) for simulations of sediment transport at the same geographic location. The median floc sizes measured by the LISST were used in the simulations.

Numerical runs used a fast relaxation-time method recently implemented in the model that generates a current profile with a user-defined depth-averaged velocity (chosen here to match the observed velocity profile). The oscillatory part of the flow was described using a representative sinusoidal wave with the observed spectral

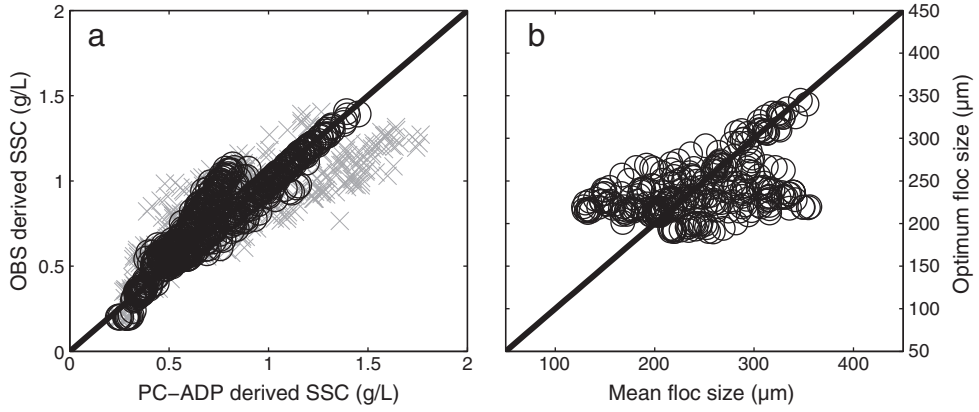

Fig. 6. Correlation between (a) measured (OBS) and estimated (PC-ADP) suspended sediment concentration (gray "x"s: estimates using mean floc size, black circles: estimates using optimum floc size), (b) optimum floc size (providing the best SSC estimates with the OBS measurements at 50 and 75 cmab) and mean floc size (measured by the LISST at 120 cmab).

peak frequency and orbital velocity amplitude calculated using linear wave theory. This allowed for multiple tests with different roughness heights at the bed and the resuspension coefficients (varied in the runs between 10^{-7}–10^{-4}).

The profiles of SSC and current velocity shown in Fig. 7a and b are calculated based on the optimal (k_s,γ_0) pair, i.e., the values that yield the best agreement between the calculated and the PC-ADP derived vertical profiles of SSC. The normalized RMS error for simulated SSC profiles is 11%, and for current speed profiles 7%, on average. The results support the assumption that SSC profiles derived from acoustic backscatter can help improve numerical model results and implicitly model estimates of quantities that are difficult to observe directly, such as the near-bed turbulent stress field.

5. Results

Fig. 7a shows an example of two profiles corresponding to two different mean floc sizes (250 μm, and 160 μm) but with the same SSC = 4 g/L at approximately 12 cmab. The vertical profiles are in agreement with the conclusions of previous studies on that smaller flocs, for similar flow conditions, result in higher SSC in the upper water column with more mixed profile (Dyer and Manning, 1999; Safak et al., 2010). According to Eq. (8), the settling velocity scales with $D_f^{3-n_f}$. Hence, with a typical fractal dimension of around 2, settling velocity increases almost linearly with floc size. Larger flocs settle faster, thus leading to lower concentrations in the upper column. The dependency shown in Fig. 7a was consistently observed through the entire measurement points analyzed. This process was investigated in more detail with the numerical results and the gradient Richardson number (Ri) profiles for sediment-induced stratification,

$$Ri = -\frac{(\sigma-1)g\frac{\partial\phi}{\partial z}}{\left(\frac{\partial u}{\partial z}\right)^2+\left(\frac{\partial v}{\partial z}\right)^2}, \tag{9}$$

with σ the specific gravity, ϕ the volume concentration of the sediment floc, u and v the horizontal components of the velocity. While numerical simulation results for the two cases shown in Fig. 7 exhibit vertical profiles of velocity that are qualitatively similar (Fig. 7b), the computed gradient Richardson number differs sharply (Fig. 7c). For the case of smaller floc (triangles and thin lines with floc size of 160 μm), Ri near the bed is around 0.2 and increases upward. On the other hand, for the case of larger floc (circles and thick lines with floc size of 250 μm), the near bed Ri value is much larger (around 0.68). However, it first decreases to 0.5 at around $z = 5$ cm above the bed and then increases with distance from the bed but at a lower rate compared to that of smaller floc size. The turbulent intensity ($\sqrt{2 * TKE}$, where TKE is the turbulent kinetic energy) profiles normalized by the friction velocities are seen in Fig. 7d. Based on these profiles, it is clear that although the case of larger floc is more energetic, relatively high turbulence only exists within the first 5 cm above the bed, which is approximately associated with the wave boundary layer thickness. Above the wave boundary layer, the normalized turbulence intensity decreases significantly.

6. Discussion

One source of uncertainty in this study is the limited availability of information about sediment size distribution. The LISST functionality is limited in the relatively high near-bed concentrations, and can be deployed only at locations (high in the water column) where the concentration is expected to be low. However, it is very likely that floc size varies throughout the water column due to varying turbulence intensity and sediment availability, both of which are relatively high near the bed (Dyer and Manning, 1999; Hill et al., 2001; Winterwerp, 2002, and many others). This would require the investigation on the relationship between flocculation, sediment concentration and turbulent flow that is at this time beyond our instrument capabilities. An intermediate step toward evaluating this three-way interaction is currently being taken based on field data collected over the Atchafalaya Shelf during similar flow conditions and the findings will be presented elsewhere (Safak et al., 2012).

For the field application presented here, the floc size was assumed to be independent of the vertical coordinate throughout the PC-ADP profiling range. We stress that this constraint is not an algorithm limitation, but rather a matter of simplicity and convenience, and matches the behavior of the numerical model (see Section 4.1). More importantly, it is imposed in the context of a general lack of field observations about the specifics of floc dynamics (e.g., unknown floc fractal dimension or; the single-point size data collected at 120 cmab, outside the PC-ADP profiling range). While the assumption of vertically-constant floc size is probably unrealistic, the results can be interpreted as an effective-size value. Only the vertical variability was discarded; the time-variability of the floc size was taken into account (Fig. 2f). It is remarkable that, despite the limitations imposed on floc size, the optimization search space is large enough to allow a good agreement between the OBS-3 observations and the SSC values estimated from backscatter (Figs. 5b and c, 6a).

Whether one should use flocs or primary particles as scatterers is a difficult question. Even for a laboratory environment, the requirement of controlling the floc size implies simultaneously controlling delicate aspects of floc dynamics such as the settling velocity, concentration and flow turbulence. Previous studies in muddy environments offer no clear guidance on whether the acoustic backscatter responds to

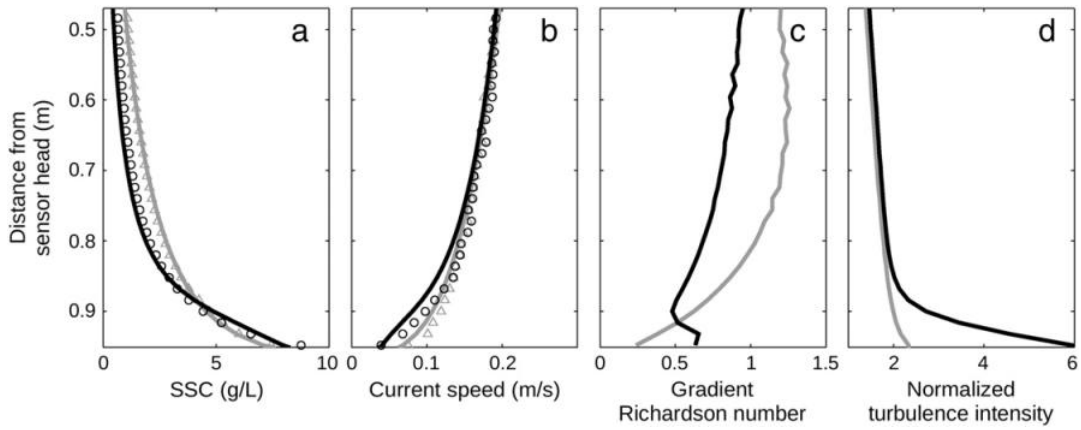

Fig. 7. (a) Two observed SSC vertical profiles (estimated from acoustic backscatter) (circles: 250 μm, March 8th at 21:00 h UTC; and triangles: 160 μm, March 4th at 18:30 h UTC), and corresponding model simulations (thick line: 250 μm and thin line: 160 μm). (b) Corresponding observed and simulated current speeds. Vertical profiles of: (c) the Richardson number; (d) the normalized turbulence intensity obtained from numerical simulations.

flocs (regarded as single larger particles), or to primary constituent particles. For example, Fugate and Friedrichs (2002) suggested that the acoustic response for resuspended aggregates depends mostly on the constituent grains rather than the floc characteristics. Gartner (2004), however, estimated successfully SSC profiles by using flocs as scatterers. Moreover, Ha et al. (2011) confirmed that PC-ADP backscatter does not invert well for grain sizes of order of 1 μm, and likely responds to flocs. The relative importance of absorption components ξ_s (Eq. (4)) and ξ_v (Eq. (5)) depends strongly on the particle size. At 1.5 MHz (the frequency of the signal transmitted by the acoustic profiler used in this study), ξ_s dominates the sediment attenuation for large particles ($\alpha > 100$ μm), the range of floc size observed in this study. In contrast, primary particles are typically small ($a \approx 5$ μm) compared to the acoustic wavelength ($ka = 0.015$), and in this range, ξ_v becomes important (Urick, 1948; Ha et al., 2011). To avoid biasing the calculations toward either ends of the particle size distribution, both of the absorption components ξ_s and ξ_v (i.e., floc and primary particle contributions) were taken into account in this study. However, inversion calculations conducted using alternatively flocs and primary particles as scatterers consistently show better agreement for flocs, with a marginally significant correction due to primary-particle viscous effect.

The approach to calculate SSC from backscatter has shown limitations and ambiguities in previous applications. Single-frequency instruments cannot distinguish particle-size from SSC variability (Gartner, 2004). The acoustic backscatter has maxima for (thus is biased toward) certain geometries and suspended particles. Air-bubble backscatter dominates that of sediment particles of same size (Libicki et al., 1989; Hamilton et al., 1998; Traykovski et al., 2007); most efficient backscatter is achieved for particles with $ka = O(1)$. The shape of the scattering particles is not important if $ka \ll 1$ (Rayleigh scattering regime; Thorne and Meral, 2008), but becomes so as ka approaches unity. The application of the method in mud dominated environments adds more complexities. For example, vertical variation of the sediment size (mud flocs) is much more significant than sandy environments, since aggregation and floc break-up can take place immediately depending on flow conditions (e.g., turbulence level). In use of single frequency instruments, this significant change in floc size can be interpreted as a change in sediment concentration. These ambiguities constrain our ability to fully represent floc dynamics, and our interpretation of the results.

A closer examination of the structure of the current boundary layer suggests that the transition to a larger SSC gradient with the depth is associated with a critical change in sediment-induced density stratification. For similar flow conditions, decreasing floc size, i.e., decreasing settling velocity decreases near-bed suspended sediment concentration, produces a well-mixed concentration profile (Fig. 7a). For smaller flocs, *Ri* near the bed is low then increases with height above the bed. For larger flocs, *Ri* near the bed is higher and then increases upwards with a slower rate than that of the smaller floc case (Fig. 7c). This behavior can be explained analytically based on steady channel flow. Although the conditions are more complicated here due to effect of waves, the wave-averaged process can be explained qualitatively.

Assume, for simplicity, a log–law $u(z) = \frac{u_*}{\kappa} ln\frac{z}{z_0}$, for turbulent boundary layer (u_* is the friction velocity, κ is Von Karman constant and $z_0 = k_s/30$) and the Rouse profile for sediment concentration

$$\phi = \phi_r \left(\frac{h-z}{z}\right)^{\gamma}, \tag{10}$$

(ϕ_r is a reference concentration, h is the depth of flow, $\gamma = \frac{w_s}{\beta_r \kappa u_*}$ is the Rouse number where β_r is the ratio between eddy diffusivity and sediment diffusivity, assumed $\beta_r = 1$). Substituting the last two expressions into Eq. (9), yields

$$Ri = (\sigma - 1) g \phi_r \frac{w_s}{u_*^3} \kappa h \left(\frac{h-z}{z}\right)^{\gamma-1}. \tag{11}$$

This result highlights the critical effect of γ on the *Ri* profile.

For $\gamma < 1$, this expression predicts $Ri(z)$ increasing with the height above the bed. Based on $\gamma \propto \frac{w_s}{\kappa u_*}$, this case corresponds to small settling velocity and/or strong currents, and is implicitly associated with dilute suspensions. In this case, values of $Ri < 0.25$ are observed near the bed, and damping of turbulence due to sediment-induced stratification is small.

For $\gamma > 1$, $Ri(z)$ decreases with z. Near-bed *Ri* can be larger than 0.25; damping of turbulence due to sediment induced stratification is important. This case corresponds to large settling velocity and/or weak currents. Implicitly, sediment accumulates near the bed, where concentrations are high.

In the examples shown in Fig. 7, flow conditions are similar, but the difference in the size of the flocs is apparently enough to cause the significant difference in *Ri* profiles. Rouse numbers corresponding to the small-floc and large-floc cases are $\gamma = 0.62$ ($u_* = 0.94$ cm/s, $w_s = 0.24$ cm/s) and $\gamma = 0.86$ ($u_* = 1.27$ cm/s, $w_s = 0.45$ cm/s), respectively. Here, our estimate of Rouse number does not explicitly account for the effect of sediment on damping the turbulence, such as through a reduced Karman constant κ. However, qualitatively the case with larger floc has a Rouse number that is significantly larger than that of smaller floc. Hence, the large-floc case shows a near-bed *Ri* value around 0.6, indicating that the damping of turbulence due to sediment induced stratification is important.

7. Summary and conclusions

A new method for estimating the vertical profile of suspended sediment concentration is used to re-examine the relationship between sediment stratification and floc size in muddy environments. Acoustic backscatter is converted here to SSC estimates using an algorithm that extends to cohesive sedimentary environments a method originally developed for sand (Holdaway et al., 1999; Thorne and Hanes, 2002). The procedure evaluates an instrument constant using an inverse method that seeks to minimize the error between the estimates and independent measurements (e.g., optical) at a small number of spatial points. The algorithm is validated using measurements of flow and backscatter intensity from an acoustic profiler (PC-ADP), optical measurements (OBS-3) of SSC, and grain-size distribution observations (LISST) collected in 2006 on the muddy inner shelf fronting the Atchafalaya Bay, Louisiana, USA. Differences between estimated profiles and optical measurements can be attributed to limitations of the method, most of them related to yet unresolved physics of the interaction between sound and the fractal geometry of cohesive sediment flocs.

The assumption that the floc size is independent of height is probably the strongest specific constraint imposed on the algorithm proposed here. However, this is in essence an acknowledgment of factors that are beyond the scope of this study: the floc-size/concentration ambiguity associated with single-frequency acoustic observations; lack of direct observations of vertical variability of floc size; numerical modeling constraints. In principle, this constraint can be removed by using data collected with a multi-frequency instrument, by implementing the flocculation models into boundary layer models (e.g., Winterwerp, 2002) or when more adequate sediment size observations become available with higher resolution. In the absence of these elements, the assumption of vertically-uniform floc still produces vertical SSC profiles that agree well with optical point measurements, suggesting that the physics may be dominated by sediment concentration rather than sediment size distribution at this location and the method is robust enough for applications.

While "field observations" of SSC profiles are in general useful for the study of sediment transport, they become an essential piece of information when coupled with numerical models. A complete description of cohesive sediment transport involves a large number of physical quantities, such as the floc size, or the fractal-dimension of the flocs, that are often difficult to measure directly. Inverse modeling

procedures allow one to estimate their values based on the overall performance of the model, but accurate and sufficient data is then necessary to produce well-constrained simulations. For example, a numerical model can match a single-point SSC measurement using a wide range of floc sizes (Safak et al., 2010). However, the outcome is a range of sediment stratification configurations, possibly spanning different interpretations of flow–sediment interaction. Estimates of SSC profiles based on observations eliminate this ambiguity.

Here, we used the observed SSC profiles to constrain a one-dimensional bottom boundary layer model, and used the numerical simulations to investigate the relationship between sediment stratification and temporal floc size variability. Observed SSC profiles with similar near-bed (~10–15 cmab) concentrations but corresponding to different floc-sizes confirm the trend (hypothesized by Dyer and Manning, 1999, based on laboratory and field observations, and by Safak et al., 2010 based on numerical simulations) that low concentrations promote flocculation (high in the water column), and sediment stratification increases with the floc size. Numerical simulations show that a critical transition in the profile of gradient Richardson number can occur, related to increased damping of flow turbulence by sediment induced density stratification. This supports previously published numerical results (Safak et al., 2010).

Acknowledgments

This research was supported by the Office of Naval Research funding of contracts N00014-10-1-0363 and N00014-11-1-0269. The corresponding author acknowledges the Council of Higher Education, Turkey and the Yildiz Technical University for the scholarship offered during his doctoral study. The authors are grateful to Prof. Ashish J. Mehta for his valuable suggestions and advice about mud dynamics. We thank the two anonymous reviewers and the Editor Dr. John T. Wells for their insightful and constructive comments that improved the manuscript.

References

Allison, M.A., Kineke, G.C., Gordon, E.S., Goni, M.A., 2000. Development and reworking of a seasonal flood deposit on the inner continental shelf off the Atchafalaya River. Continental Shelf Research 20, 2267–2294.

Allison, M.A., Sheremet, A., Goni, M.A., Stone, G.W., 2005. Storm layer deposition on the Mississippi–Atchafalaya subaqueous delta generated by Hurricane Lili in 2002. Continental Shelf Research 25, 2213–2232.

Betteridge, K.F.E., Thorne, P.D., Cooke, R.D., 2008. Calibrating multi-frequency acoustic backscatter systems for studying near-bed suspended sediment transport processes. Continental Shelf Research 28, 227–235.

Crawford, A.M., Hay, A.E., 1993. Determining suspended sand size and concentration from multifrequency acoustic backscatter. Journal of the Acoustical Society of America 6, 2247–2254.

Downing, A., Thorne, P.D., Vincent, C.E., 1995. Backscattering from a suspension in the near field of a piston transducer. Journal of the Acoustical Society of America 97 (3), 1614–1620.

Dyer, K.R., Manning, A.J., 1999. Observation of the size, settling velocity and effective density of flocs, and their fractal dimensions. Journal of Sea Research 41, 87–95.

Francois, R.E., Garrison, G.R., 1982a. Sound absorption based on ocean measurements. Part I: pure water and magnesium sulfate contributions. Journal of the Acoustical Society of America 72, 896–907.

Francois, R.E., Garrison, G.R., 1982b. Sound absorption based on ocean measurements. Part II: boric acid contribution and equation for total absorption. Journal of the Acoustical Society of America 72, 1879–1890.

Fugate, D.C., Friedrichs, C.T., 2002. Determining concentration and fall velocity of estuarine particle populations using ADV, OBS and LISST. Continental Shelf Research 22, 1867–1886.

Gartner, J.W., 2004. Estimating suspended solids concentrations from backscatter intensity measured by acoustic Doppler current profiler in San Francisco Bay, California. Marine Geology 211, 169–187.

Ha, H.K., Maa, J.P.-Y., Park, K., Kim, Y.H., 2011. Estimation of high-resolution sediment concentration profiles in bottom boundary layer using pulse-coherent acoustic Doppler current profiles. Marine Geology 279 (2011), 199–209.

Hamilton, L.J., Shi, Z., Zhang, S.Y., 1998. Acoustic backscatter measurements of estuarine suspended cohesive sediment concentration profiles. Journal of Coastal Research 14 (4), 1213–1224.

Hay, A.E., Sheng, J., 1992. Vertical profiles of suspended sand concentration and size from multifrequency acoustic backscatter. Journal of Geophysical Research 97, C10. http://dx.doi.org/10.1029/92JC01240.

Hill, P.S., Voulgaris, G., Trowbridge, J.H., 2001. Controls on floc size in a continental shelf bottom boundary layer. Journal of Geophysical Research 106 (C5), 9543–9549.

Hoitink, A.J.F., Hoekstra, P., 2005. Observations of suspended sediment from ADCP and OBS measurements in a mud-dominated environment. Coastal Engineering 52, 103–118.

Holdaway, G.P., Thorne, P.D., Flatt, D., Jones, S.E., Prandle, D., 1999. Comparison between ADCP and transmissometer measurements of suspended sediment concentration. Continental Shelf Research 19, 421–441.

Hsu, T.-J., Traykovski, P.A., Kineke, G.C., 2007. On modeling boundary layer and gravity-driven fluid mud transport. Journal of Geophysical Research 112, C04011. http://dx.doi.org/10.1029/2006JC003719.

Hsu, T.-J., Ozdemir, C.E., Traykovski, P.A., 2009. High-resolution numerical modeling of wave-supported gravity-driven mudflows. Journal of Geophysical Research 114, C5. http://dx.doi.org/10.1029/2008JC005006.

Jaramillo, S., Sheremet, A., Allison, M.A., Reed, A.T., Holland, K.T., 2009. Wave–mud interactions over the muddy Atchafalaya subaqueous clinoform, Louisiana, USA: wave-driven sediment transport. Journal of Geophysical Research 114, C04002. http://dx.doi.org/10.1029/2008JC004821.

Kaye, G.W.C., Laby, T.H., 1986. Tables of Physical and Chemical Constants. Longman, UK, p. 477.

Khelifa, A., Hill, P.S., 2006. Models for effective density and settling velocity of flocs. Journal of Hydraulic Research 44 (3), 390–401. http://dx.doi.org/10.1080/00221686.2006.9521690.

Kranenburg, C., 1994. On the fractal structure of cohesive sediment aggregates. Estuarine, Coastal and Shelf Science 39, 451–460.

Libicki, C., Bedford, K.W., Lynch, J.F., 1989. The interpretation and evaluation of a 3-MHz acoustic backscatter device for measuring benthic boundary layer sediment dynamics. Journal of the Acoustical Society of America 85 (4), 1501–1511.

Lynch, J.F., Gross, T.F., Brumley, B.H., Filyo, R.A., 1991. Sediment concentration profiling in HEEBLE using a 1-MHz acoustic backscatter system. Marine Geology 99, 361–385.

Mossa, J., 1996. Sediment dynamics in the lowermost Mississippi River. Engineering Geology 45, 457–479.

Neill, C.F., Allison, M.A., 2005. Subaqueous deltaic formation on the Atchafalaya Shelf, Louisiana. Marine Geology 214, 411–430.

Phillips, O.M., 1958. The equilibrium range in the spectrum of wind-generated waves. Journal of Fluid Mechanics 4, 426–434.

Safak, I., Allison, M.A., Sheremet, A., 2012. Floc variability under changing turbulent stresses and sediment availability on a wave-energetic muddy shelf. Continental Shelf Research. http://dx.doi.org/10.1016/j.csr.2012.11.015.

Safak, I., Sheremet, A., Allison, M.A., Hsu, T.J., 2010. Bottom turbulence on the muddy Atchafalaya Shelf, Louisiana, USA. Journal of Geophysical Research 115. http://dx.doi.org/10.1029/2010JC006157.

Safak, I., Sahin, C., Kaihatu, J.M., Sheremet, A., 2012. Modeling wave–mud interaction on the central Chenier-plain coast, western Louisiana Shelf, USA. Ocean Modelling. http://dx.doi.org/10.1016/j.ocemod.2012.11.006.

Sahin, C., Safak, I., Sheremet, A., Mehta, A.J., 2012. Observations on cohesive bed reworking by waves: Atchafalaya Shelf, Louisiana. Journal of Geophysical Research 117. http://dx.doi.org/10.1029/2011JC007821.

Sheng, J., Hay, A.E., 1988. An examination of the spherical scatter approximation in aqueous suspensions of sand. Journal of the Acoustical Society of America 83, 598–610.

Sheremet, A., Mehta, A.J., Liu, B., Stone, G.W., 2005. Wave–sediment interaction on a muddy inner shelf during Hurricane Claudette. Estuarine, Coastal and Shelf Science 63, 225–233.

Son, M., Hsu, T.-J., 2011. The effects of flocculation and bed erodibility on modeling cohesive sediment resuspension. Journal of Geophysical Research 116, C03021. http://dx.doi.org/10.1029/2010JC006352.

Thorne, P.D., Hanes, D.M., 2002. A review of acoustic measurement of small-scale sediment processes. Continental Shelf Research 22, 603–632.

Thorne, P.D., Meral, R., 2008. Formulations for the scattering properties of suspended sandy sediments for use in the application of acoustics to sediment transport processes. Continental Shelf Research 28, 309–317.

Thorne, P.D., Hardcastle, P.J., Soulsby, R.L., 1993. Analysis of acoustic measurements of suspended sediments. Journal of Geophysical Research 98 (C1), 899–910.

Thosteson, E.D., Hanes, D.M., 1998. A simplified method for determining sediment size and concentration from multiple frequency acoustic backscatter measurements. Journal of the Acoustical Society of America 104 (2), 820–830.

Traykovski, P., Wiberg, P.L., Geyer, W.R., 2007. Observations and modeling of wave-supported sediment gravity flows on the Po prodelta and comparison to prior observations from the Eel shelf. Continental Shelf Research 27, 375–399.

Urick, R.J., 1948. The absorption of sound in irregular particles. Journal of the Acoustical Society of America 20 (3), 283–289.

Winterwerp, J.C., 2001. Stratification effects by cohesive and non-cohesive sediment. Journal of Geophysical Research 106 (C10), 22,559–22,574. http://dx.doi.org/10.1029/2000JC000435.

Winterwerp, J.C., 2002. On the flocculation and settling velocity of estuarine mud. Continental Shelf Research 22, 1339–1360. http://dx.doi.org/10.1016/S0278-4343(02)00010-9.